IEEE Access
Multidisciplinary | Rapid Review | Open Access Journal

Received December 29, 2020, accepted December 31, 2020, date of publication January 5, 2021, date of current version January 13, 2021.

Digital Object Identifier 10.1109/ACCESS.2021.3049183

Kerr-Raman Optical Frequency Combs in Silica Microsphere Pumped Near Zero Dispersion Wavelength

ELENA A. ANASHKINA AND ALEXEY V. ANDRIANOV
Institute of Applied Physics of the Russian Academy of Sciences, 603950 Nizhny Novgorod, Russia
Corresponding author: Elena A. Anashkina (elena.anashkina@ipfran.ru)

This work was supported in part by the Russian Science Foundation, (theoretical and experimental investigation of optical frequency comb (OFC) generation), under Grant 20-72-10188, and in part by the Mega-grant of the Ministry of Science and Higher Education of the Russian Federation, (development of the testbed for study of microresonators), under Contract 14.W03.31.0032.

ABSTRACT Optical frequency combs generated in whispering gallery mode microresonators are in high demand for basic science and a large number of applications including telecommunication systems and quantum optics. Here, we study experimentally and theoretically optical frequency comb generation in a silica microsphere with a zero dispersion wavelength near 1.55 μm pumped by a continuous wave laser widely tunable in the C-band. We considered the optical frequency comb generation for a pump wavelength in a normal dispersion region, in a low anomalous dispersion region, and very close to the zero dispersion wavelength. Kerr-assisted and Raman-assisted (Stokes) combs as well as anti-Stokes combs emerging due to the four-wave mixing between the Kerr and Raman combs are attained in experiments. The mechanisms of producing individual peaks of optical frequency combs are verified in numerical simulations. A 270-nm optical frequency comb covering the telecommunication E-, S-, C-, L-, U-bands and further up to 1.7 μm is also demonstrated.

INDEX TERMS Optical frequency comb (OFC), Kerr-assisted OFC, Raman-assisted OFC, silica microsphere, whispering gallery mode resonator (WGMR).

I. INTRODUCTION

Optical frequency combs (OFCs) produced in whispering gallery mode microresonators (WGMRs) are demanded in basic science and in a huge number of applications, including advanced telecommunication systems [1], [2] and quantum optical communication [3], [4], and can lead to great advances in the entangled states generation for quantum computation [5]. The currently available technologies allow manufacturing high Q-factor WGMRs of different shapes based on various materials [6]–[13]. On-chip WGMRs have been intensively developed and investigated [6], but silica microspheres (MSs) are also a very convenient platform for studying nonlinear phenomena and demonstrating proof-of-concepts as they can be easily produced from standard optical fibers, their dispersion can be controlled by choosing their diameters, and the nonlinear dynamics of intracavity radiation for them can be described as for other WGMR types in the framework of the Lugiato-Lefever equation (LLE) [6]. Many regimes of OFC generation achieved in on-chip WGMRs were also investigated in silica MSs and even observed for the first time, which enabled a significant progress in understanding nonlinear physics or discovering new effects. For example, Raman lasing was first demonstrated in a silica MS [14] and after that investigated on the basis of this and other platforms [15]–[22]. Kerr and Kerr-Raman OFCs generation was also investigated experimentally in a silica MS [16]. Experimental Kerr-assisted and Raman-assisted OFCs generation in a silica microbottle WGMR was reported in [17]. Raman-assisted Kerr frequency combs were reported with barium fluoride and strontium fluoride WGMRs in the normal dispersion region [23], [24]. The generation on Raman-Kerr frequency combs in normal dispersion regime was also investigated numerically in [25].

Here, we study experimentally and numerically the generation of Kerr-assisted and Raman-assisted (Stokes) OFCs, as well as the generation of anti-Stokes OFCs emerging due to the four-wave mixing (FWM) between the spectral

The associate editor coordinating the review of this manuscript and approving it for publication was Derek Abbott.

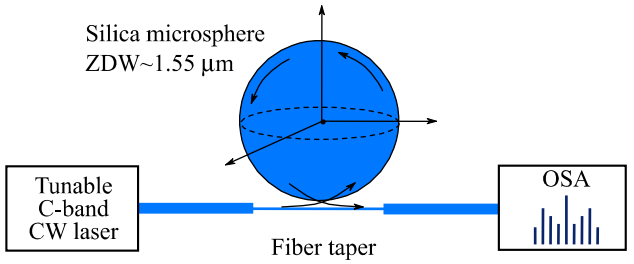

FIGURE 1. A simplified scheme of the experimental setup.

components near the pump wavelength and the Stokes components in a silica MS for different dispersion regimes. By tuning a wavelength of a continuous wave (CW) pump laser, we investigate the regimes of OFC generation for a pump wavelength λ_p in a normal dispersion region ($\lambda_p <$ ZDW), in slightly anomalous dispersion regions ($\lambda_p >$ ZDW), and very close to ZDW ($\lambda_p \approx$ ZDW). By switching on and switching off the Raman response in modeling, we confirm that certain Stoke spectral peaks originate from the Raman effect and the anti-Stokes ones originate from FWM. The calculated phase matching conditions also explain the nature of the observed anti-Stokes spectral harmonics or their absence.

II. RESULTS AND DISCUSSION

The experimental scheme is shown in Figure 1(a). It consists of a silica MS with an optimized diameter of 162 μm for obtaining the ZDW near 1.55 μm. The MS was made of a standard single-mode telecommunication fiber SMF28e using the purposely designed programs for the Fujikura ARCMaster FSM-100P+ fiber splicer as in our previous work [15]. The MS with a measured Q-factor of $5{\cdot}10^7$ was pumped by a CW laser widely tunable in the C-band (Pure Photonics, PPCL550-180-60, 60 nm tuning range, 10 kHz linewidth). Coupling of pump light and outcoupling of the generated OFCs were arranged with a fiber taper. The description of producing MS and fiber taper as well as other experimental details are available in [12], [15]. The spectra of output signals were recorded by OSA (Optical Spectrum Analyzer, Yokogawa AQ6370D).

To optimize the ZDW and find the required size of the silica MS, we calculated dispersion β_2 for different radii R using the approach based on numerical solution of a characteristic equation [26] as in our previous works [27], [28]. We found eigenfrequencies ν_l for the fundamental transverse electric mode families, where l is the azimuthal mode index, and after that we calculated β_2 as follows [29], [30]:

$$\beta_2 = -\frac{1}{4\pi^2 R}\frac{\Delta(\Delta\nu_l)}{(\Delta\nu_l)^3}, \tag{1}$$

where

$$\Delta\nu_l = \frac{\nu_{l+1}-\nu_{l-1}}{2};\ \Delta(\Delta\nu_l) = \nu_{l+1} - 2\nu_l + \nu_{l-1}. \tag{2}$$

The corresponding wavelength dependences of dispersion are plotted in Figure 2(a) for different R. The required ZDW of 1.55 μm is obtained for the MS diameter $2R = 162$ μm.

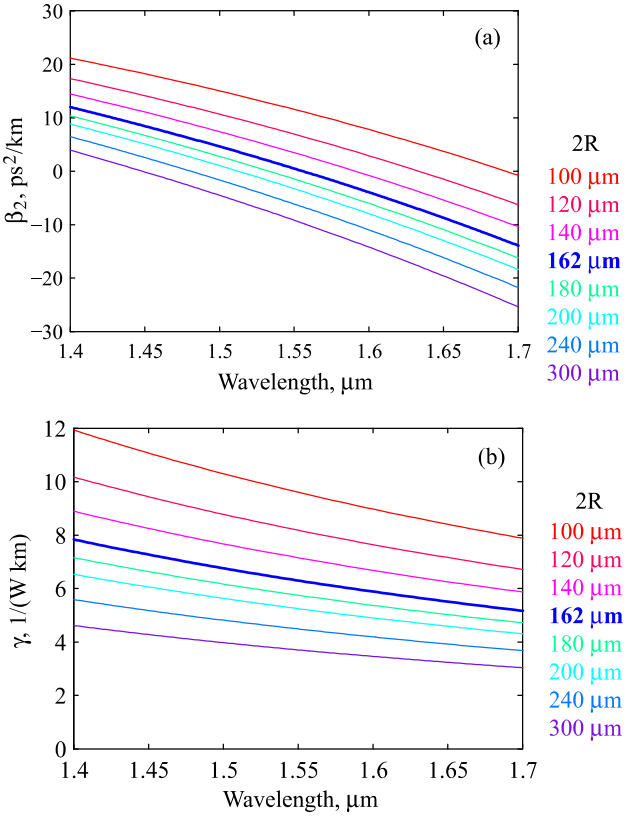

FIGURE 2. Dispersion (a) and nonlinear Kerr coefficients (b) as a function of wavelength for the fundamental TE modes calculated for microspheres of different diameters. The bold blue lines correspond to the microsphere with a diameter of 162 μm used in the experiments.

We also estimated nonlinear Kerr coefficients γ as a function of wavelength λ using the approximate formula from the work [31]:

$$\gamma = \frac{2\pi n_2}{\lambda}\frac{2\pi R}{3.4\pi^{3/2}\left(\frac{\lambda}{2\pi n}\right)^3 l^{11/6}} \tag{3}$$

where n and n_2 are the linear and nonlinear refractive indices, respectively. The nonlinear Kerr coefficients found for different radii are plotted in Figure 2(b).

The nonlinear dynamics of an intracavity field leading to OFC generation was simulated numerically in the framework of the LLE [6], [32] as in [28], [33] using home-made software based on the Split-step Fourier method. We used the master equation in the following form [6], [29], [34]:

$$t_R\frac{\partial E(t,\tau)}{\partial t} = \sqrt{\theta}E_{in} - 2\pi R\left(\frac{i\beta_2}{2}\frac{\partial^2}{\partial\tau^2} - \frac{\beta_3}{6}\frac{\partial^3}{\partial\tau^3}\right)E, + \left(2\pi\, iR\gamma_p\int R(s)|E(t,\tau-s)|^2 ds - \alpha - i\delta_p\right)E \tag{4}$$

where $E(t,\tau)$ is the intracavity field; τ and t are the fast and slow times; $t = N{\cdot}t_R$; $t_R = 2\pi Rn/c$ is the microresonator roundtrip time, N is the microresonator roundtrip number; δ_p is the phase detuning of the pump field E_{in} from the nearest

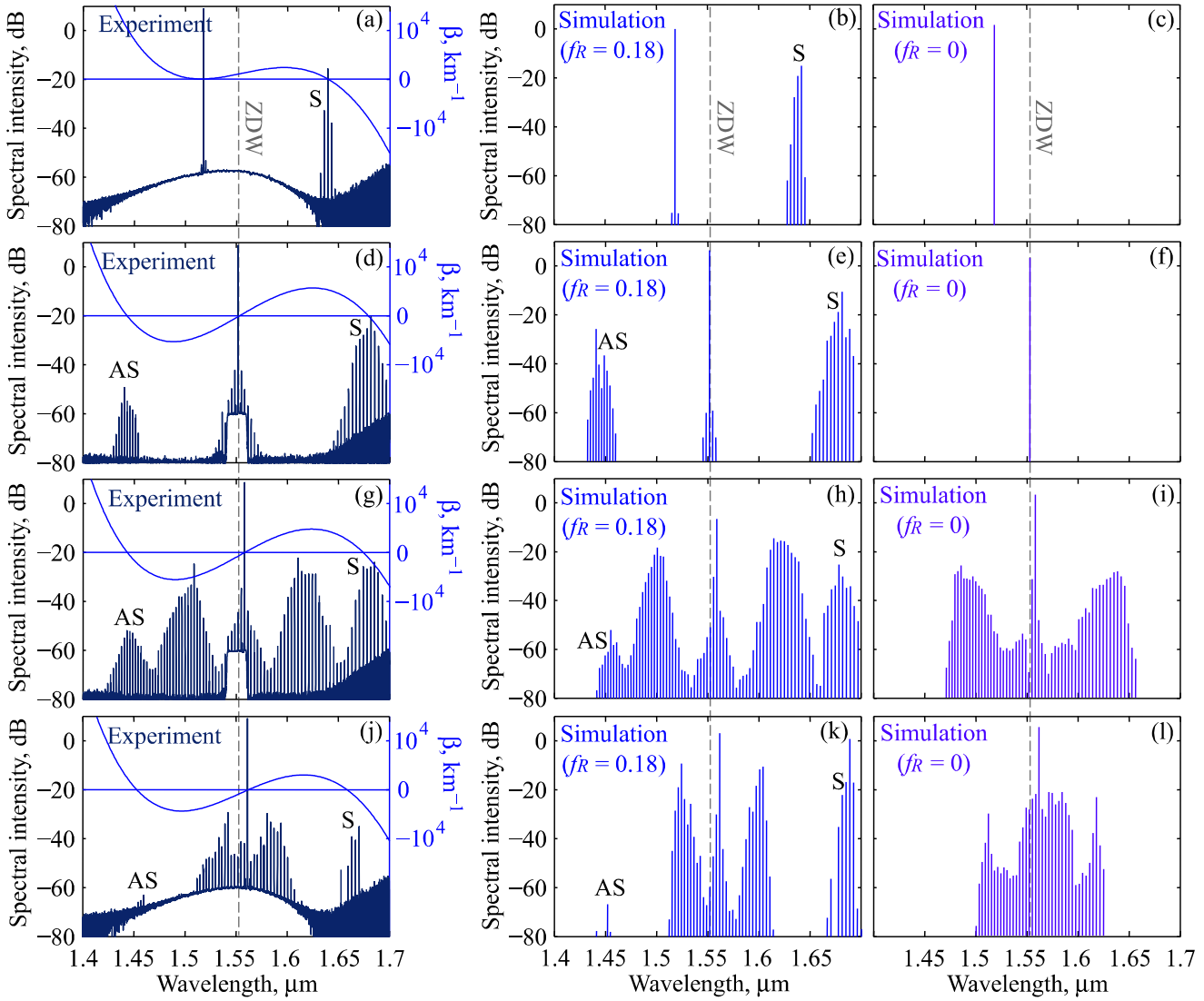

FIGURE 3. Optical spectra: experimental (a,d,g,j; left axes), simulated taken into account the Raman contribution (b,e,h,k) and simulated without allowance for Raman gain (c,f,i,l). Propagation constants β for demonstration of phase matching conditions between Raman-assisted Stokes ("S") and anti-Stokes ("AS") waves (a,d,g,j; right axes). Vertical dashed lines indicate calculated ZDW. (a,b,c) $\lambda_p = 1.518\mu$m in the normal dispersion range; (d,e,f) $\lambda_p = 1.552$ μm near ZDW; (g,h,i) $\lambda_p = 1.558\mu$m in the slightly anomalous dispersion range; (j,k,l) $\lambda_p = 1.562$ μm in the anomalous dispersion range with a higher absolute value in comparison with (g,h,i).

resonance; θ is the transmission coefficient of the input and output coupler; $\beta_k = d^k\beta/d\omega^k$ are the Taylor series expansion coefficients of the propagation constant $\beta(\omega)$ taken at the pump frequency ω_p in the retarded frame; $\alpha = (2\pi)^2 R/(Q\lambda_p)$ is the loss coefficient as the sum of coupling and intrinsic losses; γ_p is the nonlinear Kerr coefficient at ω_p (it is seen from Figure 2(b) that the frequency dependence of γ on λ is weak enough and can be neglected here). We took into account β_2 and β_3 since in the considered wavelength range, where the interplay between the first-order Raman effects and FWM was studied, the influence of higher order dispersion terms $\beta_{k\geq 4}$ can be neglected (but the impact of $\beta_{k\geq 4}$ may be significant at the wavelengths well beyond this range [35], [36]). The nonlinear response function was taken in the commonly used form

$$R(t) = (1 - f_R)\delta(t) + f_R h_R(t), \tag{5}$$

where $\delta(t)$ is the Dirac delta function; f_R is the fractional contribution of the Raman response, and $h_R(t)$ is approximated by

$$h_R(t) = \left(\tau_1^{-2} + \tau_2^{-2}\right)\tau_1 \exp\left(-t/\tau_2\right)\sin\left(t/\tau_1\right), \tag{6}$$

with $\tau_1 = 12.2$ fs and $\tau_2 = 32$ fs [32].

To reveal the Raman impact on the OFC shape for different dispersion regimes, we modeled LLE with allowance for Raman response (setting the Raman fraction $f_R = 0.18$) and purposely without this effect ($f_R = 0$). We did not

know exactly the detuning and coupling coefficients, but we checked numerically that when these parameters were varied in a fairly wide range, the generated spectra were qualitatively similar.

The experimental spectra in comparison with the corresponding simulated ones for different dispersion regimes are shown in Figure 3(a-l), where the vertical dashed lines indicate the calculated ZDW. The Stokes spectral components obtained due to multimode Raman generation are labeled by "S" and the anti-Stokes components obtained due to FWM of the pump light with these Stokes signals are labeled by "AS".

First, we set λ_p near 1.518 μm in a normal dispersion region ($\beta_2 > 0$) and obtained multimode Raman lasing in the U-band in the absence of Kerr OFC near the pump (see Figure 3(a)). The same spectrum (Figure 3(b)) was obtained in numerical modeling. The approximate phase matching condition ($\Delta\beta = 2\beta(\lambda_p) - \beta(\lambda_S) - \beta(\lambda_{AS}) = 0$ [32]) for the anti-Stokes signal was not satisfied as seen from the graph of the function $\beta(\lambda)$ in Figure 3(a); therefore, the anti-Stokes signal was not generated. When we switched off the Raman response in the simulation, the Stokes waves vanished as expected and only λ_p remained (see Figure 3(c)). Note that, when λ_p is in the normal dispersion range, FWM gain can be possible due to the interplay between β_2 and β_4 [35], [36]. In [36] it was shown for a silica microsphere with the diameter close to the diameter of our sample and pump wavelengths in the normal dispersion range that the long-wavelength sideband generated due to FWM is a few hundreds of nm shifted from the pump wavelength.

Next, we set $\lambda_p = 1.552$ μm near the ZDW ($\beta_2 \approx 0$) and observed three spectrally separated OFCs: in the C-band near λ_p, in the U-band at the Stokes wavelength, and in the E-band at the anti-Stokes wavelength (Figure 3(d)). The experimental and the corresponding numerical results are in a good agreement (compare Figure 3(d) and (e)). The calculated function $\beta(\lambda)$ is also plotted in Figure 3(d). When we set $f_R = 0$, the Stokes and anti-Stokes components were not observed (Figure 3(f)). Furthermore, there was no Kerr comb near λ_p for $f_R = 0$ (Figure 3(f)), so the spectral lines near the pump wavelength in Figures 3(d,e) may be explained by the nonzero Raman gain at small frequencies and/or nondegenerate FWM between pump light and lines belonging to Raman OFC. Note that it was earlier demonstrated theoretically that the Raman response at small frequencies affects the OFC spectral shape at the pump frequency [28], [34].

Further, we set $\lambda_p = 1.558$ μm in the range of low anomalous dispersion ($\beta_2 < 0$). The experimental spectrum with a width of 270 nm covering the E-, S-, C-, L-, U-bands and further up to 1.7 μm is presented in Figure 3(g). There are pronounced comb humps between the OFC at λ_p and the OFC at Stokes wavelengths and between the OFC at λ_p and the OFC at anti-Stokes wavelengths (Figure 3(g)). The numerical modeling gives the same results (see Figure 3(h)). These spectral harmonics are generated due to FWM (λ_p is in the anomalous dispersion range) even in the absence of Raman gain as shown in Figure 3(i).

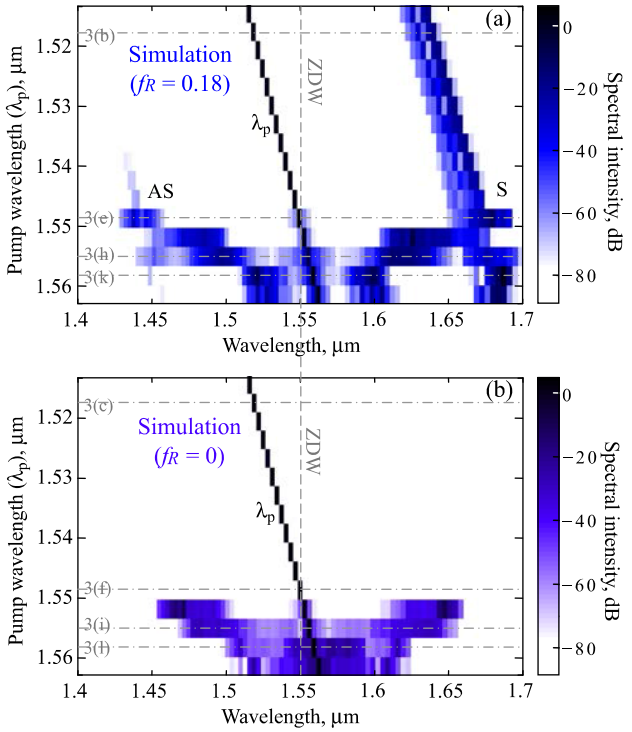

FIGURE 4. Numerically simulated spectrum evolution for varying pump wavelength when $f_R = 0.18$ (a) and $f_R = 0$ (b). Vertical dashed line indicates calculated ZDW. Horizontal dash-dotted lines indicate the corresponding regimes in Figure 3.

After that, λ_p was further tuned (up to 1.562 μm) to a slightly higher anomalous dispersion. The experimental spectrum presented in Figure 3(j) is qualitatively similar to that shown in Figure 3(g), but there are quantitative differences. The efficiency of anti-Stokes wave generation in the E-band is significantly lower due to worse phase-matching conditions. These conditions are satisfied only for the Stokes harmonics which are blue-shifted from the main Stokes line with the highest spectral intensity. The Kerr-assisted OFC generation was observed in a narrower spectral range (in the C-band and partially the S- and L-bands). These features were also confirmed by the numerical results shown in Figure 3(k). With switched off Raman gain in the simulation, Raman-assisted harmonics are not produced and the Kerr-assisted OFC is generated with a slightly different shape (compare Figure 3(k) and (l)).

Finally, we performed a more detailed numerical simulation to demonstrate the transitions between the OFC regimes shown in Figure 3 and summarize the results. Figures 4(a) and (b) demonstrate the spectra envelopes for varying λ_p when $f_R = 0.18$ and $f_R = 0$, respectively. The regimes presented in Figure 3 are shown in Figure 4 too and marked by horizontal dash-dotted lines labeled by '3(b)', '3(e)', '3(h)' etc. Note that spectral envelope is plotted (individual comb lines are not resolved) and the pump wavelength changes in steps correspond to FSR (free spectra range which is the difference between the wavelengths of the neighboring eigenmodes). When the pump wavelength is in the normal dispersion range

(λ_p < ZDW), wavelength-tunable multimode Raman lasing is achieved by tuning λ_p (see Figure 4(a), the area above dash-dotted line '3(e)'). In the slightly anomalous dispersion range (λ_p > ZDW), moving from Figure 3(d,e) to Figure 3(g,h), the humps corresponding only to FWM (between the pump and Stokes components as well as between the pump and anti-Stokes components) overlap with Stokes and anti-Stokes humps, respectively (Figure 4(a)). The fact that this is not broadening of the single Stokes (anti-Stokes) hump can be understood by comparing Figures 4(a) and 4(b), where FWM spectral components are present in the absence of Raman gain (compare the spectrum between dash-dotted lines labeled by '3(e)' and '3(h)' in Figure 4(a) with the spectrum between dash-dotted lines labeled by '3(i)' and '3(f)' in Figure 4(b)).

III. CONCLUSION

In conclusion, we studied experimentally and numerically the OFCs generation in the silica MS with the optimized diameter in different regimes depending on the pump wavelength with respect to the ZDW. We performed LLE-based numerical modeling of the OFC generation and obtained a good agreement between the experimental and numerical results, which allowed us to analyze the contribution of different nonlinear and dispersive effects to the comb structure. We confirmed that the most red-shifted OFC peak generation in the U-band and further up to 1.7 μm is governed by the Raman effect and is observed irrespective of the pump wavelength relative to the ZDW. The Raman effect plays a minor role in the generation of the central part of the OFC in the C-band and partially in the S- and L-bands, while the Kerr nonlinearity and the dispersion are the most important ones. The blue-shifted part of the OFC in the E-band is generated in the FWM process and controlled by the phase-matching condition. The most broadband OFC is generated when the pump wavelength lies in the region of small anomalous dispersion and all the above effects lead to the formation of continuous comb spectrum. In this case, we observed an OFC with a spectral width of about 270 nm in the entire frequency range, covering from the E- to the U-band and further up to 1.7 μm. We believe that the obtained results will help to further advance in understanding Kerr-Raman assisted OFC generation and may be used for the generation of OFC with tailored spectral shapes spanning from the E- to the U-bands and beyond by tuning the pump wavelength and/or ZDW, which can be easily done in a silica MS by changing the diameter.

ACKNOWLEDGMENT

(Elena A. Anashkina and Alexey V. Andrianov contributed equally to this work.)

REFERENCES

[1] P. Marin-Palomo, J. N. Kemal, M. Karpov, A. Kordts, J. Pfeifle, M. H. P. Pfeiffer, P. Trocha, S. Wolf, V. Brasch, M. H. Anderson, R. Rosenberger, K. Vijayan, W. Freude, T. J. Kippenberg, and C. Koos, "Microresonator-based solitons for massively parallel coherent optical communications," *Nature*, vol. 546, no. 7657, pp. 274–279, Jun. 2017.

[2] A. Fülöp, M. Mazur, A. Lorences-Riesgo, Ó. B. Helgason, P.-H. Wang, Y. Xuan, D. E. Leaird, M. Qi, P. A. Andrekson, A. M. Weiner, and V. Torres-Company, "High-order coherent communications using mode-locked dark-pulse kerr combs from microresonators," *Nature Commun.*, vol. 9, no. 1, Dec. 2018, Art. no. 1598.

[3] F. Monteiro, A. Martin, B. Sanguinetti, H. Zbinden, and R. T. Thew, "Narrowband photon pair source for quantum networks," *Opt. Exp.*, vol. 22, pp. 4371–4378, Feb. 2014.

[4] D. V. Strekalov, C. Marquardt, A. B. Matsko, H. G. L. Schwefel, and G. Leuchs, "Nonlinear and quantum optics with whispering gallery resonators," *J. Opt.*, vol. 18, no. 12, Dec. 2016, Art. no. 123002.

[5] P. Walther, K. J. Resch, T. Rudolph, E. Schenck, H. Weinfurter, V. Vedral, M. Aspelmeyer, and A. Zeilinger, "Experimental one-way quantum computing," *Nature*, vol. 434, no. 7030, pp. 169–176, Mar. 2005.

[6] A. Pasquazi, M. Peccianti, L. Razzari, D. J. Moss, S. Coen, M. Erkintalo, Y. K. Chembo, T. Hansson, S. Wabnitz, P. Del'Haye, X. Xue, A. M. Weiner, and R. Morandotti, "Micro-combs: A novel generation of optical sources," *Phys. Rep.*, vol. 729, pp. 1–81, Jan. 2018.

[7] A. Kovach, D. Chen, J. He, H. Choi, A. H. Dogan, M. Ghasemkhani, H. Taheri, and A. M. Armani, "Emerging material systems for integrated optical Kerr frequency combs," *Adv. Opt. Photon.*, vol. 12, pp. 135–222, Mar. 2020.

[8] B. Shen, L. Chang, J. Liu, H. Wang, Q.-F. Yang, C. Xiang, R. N. Wang, J. He, T. Liu, W. Xie, J. Guo, D. Kinghorn, L. Wu, Q.-X. Ji, T. J. Kippenberg, K. Vahala, and J. E. Bowers, "Integrated turnkey soliton microcombs," *Nature*, vol. 582, no. 7812, pp. 365–369, Jun. 2020.

[9] L. Fujii, M. Inga, J. H. Soares, Y. A. V. Espinel, T. P. M. Alegre, and G. S. Wiederhecker, "Dispersion tailoring in wedge microcavities for Kerr comb generation," *Opt. Lett.*, vol. 45, pp. 3232–3235, Jun. 2020.

[10] J. Braunfelds, R. Murnieks, T. Salgals, I. Brice, T. Sharashidze, I. Lyashuk, A. Ostrovskis, S. Spolitis, J. Alnis, J. Porins, and V. Bobrovs, "Frequency comb generation in WGM microsphere based generators for telecommunication applications," *Quantum Electron.*, vol. 50, no. 11, pp. 1043–1049, Nov. 2020.

[11] D. Bochek, N. Toropov, I. Vatnik, D. Churkin, and M. Sumetsky, "SNAP microresonators introduced by strong bending of optical fibers," *Opt. Lett.*, vol. 44, pp. 3218–3221, Jul. 2019.

[12] A. V. Andrianov, M. P. Marisova, V. V. Dorofeev, and E. A. Anashkina, "Thermal shift of whispering gallery modes in tellurite glass microspheres," *Results Phys.*, vol. 17, Jun. 2020, Art. no. 103128.

[13] A. E. Shitikov, I. A. Bilenko, N. M. Kondratiev, V. E. Lobanov, A. Markosyan, and M. L. Gorodetsky, "Billion Q-factor in silicon WGM resonators," *Optica*, vol. 5, pp. 1525–1528, Dec. 2018.

[14] S. M. Spillane, T. J. Kippenberg, and K. J. Vahala, "Ultralow-threshold Raman laser using a spherical dielectric microcavity," *Nature*, vol. 415, no. 6872, pp. 621–623, Feb. 2002.

[15] A. V. Andrianov and E. A. Anashkina, "Single-mode silica microsphere Raman laser tunable in the U-band and beyond," *Results Phys.*, vol. 17, Jun. 2020, Art. no. 103084.

[16] S. Zhu, L. Shi, L. Ren, Y. Zhao, B. Jiang, B. Xiao, and X. Zhang, "Controllable kerr and Raman-kerr frequency combs in functionalized microsphere resonators," *Nanophotonics*, vol. 8, no. 12, pp. 2321–2329, Nov. 2019.

[17] Y. Yin, Y. Niu, H. Qin, and M. Ding, "Kerr frequency comb generation in microbottle resonator with tunable zero dispersion wavelength," *J. Lightw. Technol.*, vol. 37, no. 21, pp. 5571–5575, Nov. 1, 2019.

[18] S. Kasumie, F. Lei, J. M. Ward, X. Jiang, L. Yang, and S. N. Chormaic, "Raman laser switching induced by cascaded light scattering," *Laser Photon. Rev.*, vol. 13, no. 10, Oct. 2019, Art. no. 1900138.

[19] M. Yu, Y. Okawachi, R. Cheng, C. Wang, M. Zhang, A. L. Gaeta, and M. Lončar, "Raman lasing and soliton mode-locking in lithium niobate microresonators," *Light, Sci. Appl.*, vol. 9, no. 1, Dec. 2020, Art. no. 9.

[20] Q.-F. Yang, X. Yi, K. Y. Yang, and K. Vahala, "Stokes solitons in optical microcavities," *Nature Phys.*, vol. 13, no. 1, pp. 53–57, Jan. 2017.

[21] H. Jung, Z. Gong, X. Liu, X. Guo, C.-L. Zou, and H. X. Tang, "Stokes and anti-Stokes Raman scatterings from frequency comb lines in polycrystalline aluminum nitride microring resonators," *Opt. Exp.*, vol. 27, pp. 22246–22253, Aug. 2019.

[22] Y. K. Chembo, I. S. Grudinin, and N. Yu, "Spatiotemporal dynamics of kerr-Raman optical frequency combs," *Phys. Rev. A, Gen. Phys.*, vol. 92, no. 4, Oct. 2015, 043818.

[23] G. Lin and Y. K. Chembo, "Phase-locking transition in Raman combs generated with whispering gallery mode resonators," *Opt. Lett.*, vol. 41, pp. 3718–3721, Aug. 2016.

[24] G. Lin, S. Diallo, J. M. Dudley, and Y. K. Chembo, "Universal nonlinear scattering in ultra-high Q whispering gallery-mode resonators," *Opt. Exp.*, vol. 24, pp. 14880–14894, Jun. 2016.
[25] A. V. Cherenkov, N. M. Kondratiev, V. E. Lobanov, A. E. Shitikov, D. V. Skryabin, and M. L. Gorodetsky, "Raman-Kerr frequency combs in microresonators with normal dispersion," *Opt. Exp.*, vol. 25, pp. 31148–31158, Dec. 2017.
[26] A. N. Oraevsky, "Whispering-gallery waves," *Quantum Electron.*, vol. 32, no. 5, pp. 377–400, May 2002.
[27] E. A. Anashkina, A. A. Sorokin, M. P. Marisova, and A. V. Andrianov, "Development and numerical simulation of spherical microresonators based on SiO_2–GeO_2 germanosilicate glasses for generation of optical frequency combs," *Quantum Electron.*, vol. 49, no. 4, pp. 371–376, Apr. 2019.
[28] E. A. Anashkina, M. P. Marisova, A. V. Andrianov, R. A. Akhmedzhanov, R. Murnieks, M. D. Tokman, L. Skladova, I. V. Oladyshkin, T. Salgals, I. Lyashuk, A. Sorokin, S. Spolitis, G. Leuchs, and V. Bobrovs, "Microsphere-based optical frequency comb generator for 200 GHz spaced WDM data transmission system," *Photonics*, vol. 7, no. 3, Sep. 2020, Art. no. 72.
[29] C. Milián and D. V. Skryabin, "Soliton families and resonant radiation in a micro-ring resonator near zero group-velocity dispersion," *Opt. Exp.*, vol. 22, pp. 3732–3739, Feb. 2014.
[30] S. Fujii and T. Tanabe, "Dispersion engineering and measurement of whispering gallery mode microresonator for kerr frequency comb generation," *Nanophotonics*, vol. 9, no. 5, pp. 1087–1104, Feb. 2020.
[31] V. B. Braginsky, M. L. Gorodetsky, and V. S. Ilchenko, "Quality-factor and nonlinear properties of optical whispering-gallery modes," *Phys. Lett. A*, vol. 137, nos. 7–8, pp. 393–397, May 1989.
[32] G. P. Agrawal, *Nonlinear Fiber Optics*, 6th ed. Amsterdam, The Netherlands: Elsevier, 2019.
[33] E. A. Anashkina, M. P. Marisova, A. A. Sorokin, and A. V. Andrianov, "Numerical simulation of mid-infrared optical frequency comb generation in chalcogenide As_2S_3 microbubble resonators," *Photonics*, vol. 6, no. 2, p. 55, May 2019.
[34] C. Milián, A. V. Gorbach, M. Taki, A. V. Yulin, and D. V. Skryabin, "Solitons and frequency combs in silica microring resonators: Interplay of the Raman and higher-order dispersion effects," *Phys. Rev. A, Gen. Phys.*, vol. 92, no. 3, Sep. 2015, Art. no. 033851.
[35] F. Biancalana, D. V. Skryabin, and P. S. J. Russell, "Four-wave mixing instabilities in photonic-crystal and tapered fibers," *Phys. Rev. E, Stat. Phys. Plasmas Fluids Relat. Interdiscip. Top.*, vol. 68, no. 4, Oct. 2003, Art. no. 046603.
[36] N. L. B. Sayson, K. E. Webb, S. Coen, M. Erkintalo, and S. G. Murdoch, "Widely tunable optical parametric oscillation in a Kerr microresonator," *Opt. Lett.*, vol. 42, pp. 5190–5193, Dec. 2017.

ELENA A. ANASHKINA received the B.S. and M.S. degrees in physics from the Lobachevsky State University of Nizhni Novgorod (UNN), Russia, in 2008 and 2010, respectively, and the Ph.D. degree in physics and mathematics from the Institute of Applied Physics of the Russian Academy of Sciences (IAP RAS), in 2013. She is currently a Senior Researcher with IAP RAS. Her research interests include nonlinear optics, fiber lasers, and optical microresonators.

ALEXEY V. ANDRIANOV received the B.S. and M.S. degrees in physics from UNN, in 2006 and 2008, respectively, and the Ph.D. degree in physics and mathematics from IAP RAS, in 2011. He is currently the Head of the Laboratory with IAP RAS. His research interests include fiber lasers, coherent beam combining, and optical microresonators.